Title
Error analysis for hybrid undulators

ISBN
9783954501175

Authors
Arbelaez, D
Madur, A
Marks, S
et al.

Publication Date
2011-12-01

Peer reviewed

ERROR ANALYSIS FOR HYBRID UNDULATORS*

D. Arbelaez†, A. Madur, S. Marks, S.O. Prestemon, R.D. Schlueter, LBNL, Berkeley, CA 94720, USA
H.-D. Nuhn, SLAC National Accelerator Laboratory, Menlo Park, CA 94025, USA

Abstract

A general modeling framework is introduced that allows for the solution to magnetic field perturbations due to mechanical and magnetic tolerances in hybrid undulators. For example, both geometric pole errors and permanent magnet block geometry and strength errors can be considered. Of particular significance is the scaling of the various errors with variations in the gap of the device. In this work, the perturbation analysis is presented along with specific examples of errors found in hybrid undulators.

INTRODUCTION

The analysis of magnetic field errors due to fabrication and assembly tolerances in hybrid undulators is critical to their successful application for x-ray Free Electron Lasers. This is especially true for hybrid undulators with a variable gap due to the variation in the scaling of magnetic field perturbations depending on the nature of the fabrication error. The results of this analysis will be used to determine how how the fabrication and assembly tolerances relate to the magnetic field requirements for LCLS-II (see [1]), a major upgrade to the Linear Coherent Light Source (LCLS). In this work, a perturbation model is developed to study the effect of fabrication tolerances on magnetic field errors. The approach follows the theory developed by Halbach for the analysis of insertion devices [2]. This theory has previously been applied for the study of magnetic field perturbations due to some specific undulator errors [3, 4]. Here an approach is considered that allows for the variation in the energization of a finite number of poles without being restricted to periodicity conditions over a quarter period of the device. In the following sections the perturbation analysis is presented along with some examples of specific errors found in hybrid undulators.

ANALYSIS OF HYBRID MAGNETS

In this section, an overview of the analysis of hybrid magnets composed of permanent magnet (PM) material and infinite permeability field shaping surfaces is presented. For a more detailed review of this approach, the reader is referred to the work by Schlueter [3]. In this model, the PM material is equivalently replaced by charge sheets located at appropriate surfaces on the PM block. This is an exact model for uniformly magnetized PM blocks with relative permeability, $\mu = 1$. Figure 1 shows a schematic of the approach followed in the modeling of hybrid magnets. On the left, the hybrid magnet model is shown, which is represented by two iso-scalar potential surfaces with a nearby charge, Q. Here, surface 2 is a reference surface where the scalar potential chosen to be $V = 0$ without loss of generality. A solution to this problem, which satisfies Maxwell's equations in space and has zero net flux entering surface 1 is desired. The solution to this problem can be decomposed into direct and indirect fields. The direct fields are defined as those that emanate from the charge Q and are deposited onto surfaces 1 and 2 when both surfaces are on zero scalar potential. Indirect fields are generated by the difference in scalar potential between surfaces 1 and 2 with the charge Q no longer present.

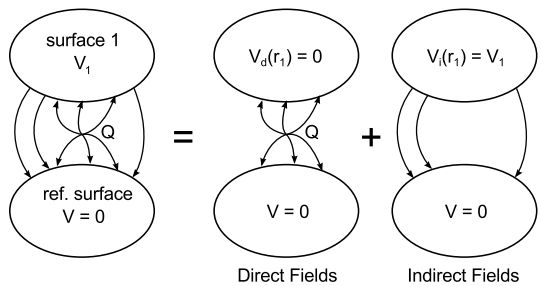

Figure 1: Hybrid magnet model consisting of constant scalar potential surfaces with a nearby charge Q.

Using the decomposition of direct and indirect fields, a solution to the hybrid magnet model can be obtained. First, the direct flux into surface 1, Φ_d^1, is obtained using the equation,

$$\Phi_d^1 = \frac{\int_{\partial\Omega_\rho} V_i(r)\rho_{eq}da}{V_i(r_1)}, \quad (1)$$

where $\partial\Omega_\rho$ is the domain on which a surface with charge density ρ_{eq} lies, and $V_i(r)$ is the solution to a boundary value problem (BVP) for the Laplace equation, $\nabla^2 V_i = 0$, with prescribed boundary conditions $V_i(r_1) = V_0$ on surface 1 and $V_i = 0$ on surface 2. Note that the choice of $V_0 \neq 0$ is arbitrary due to the linearity of the problem. For a single charge, equation 1 reduces to $QV_i(r_Q)/V_0$ where r_Q is the position of charge Q. A rigorous derivation of equation 1 can be found in [3]. The indirect flux into surface 1 can be defined as $\Phi_i^1(V_0) = -CV_0$, where C is the capacitance, which is a constant that is determined by only the geometry of the iso-scalar potential surfaces. The capacitance, $C = -\Phi_i(V_0)/V_0$, is determined by calculating the flux into surface 1, $\int_{\partial\Omega_1} \nabla V_i \cdot nda$, where V_i is the solution to the BVP, $\nabla^2 V_i = 0$, with boundary conditions

* This work was supported by the Director, Office of Science, of the US Department of Energy under Contract No. DE-AC02-05CH11231.
† darbelaez@lbl.gov

ISBN 978-3-95450-117-5

$V_i(r_1) = V_0$ (the choice of V_0 is arbitrary) on surface 1 and $V_i = 0$ on surface 2. By requiring that there be zero net flux through surface 1 (i.e. $\Phi_d^1 + \Phi_i^1 = 0$), the solution for the scalar potential on this surface is given by

$$V_1 = \frac{\Phi_d^1}{C}. \quad (2)$$

In summary, the scalar potential of the surfaces in a hybrid magnet with infinite permeability poles can be determined by: (1) solving a BVP for the Laplace equation with an arbitrary potential V_0 applied at surface 1, (2) integrating the potential over the PM material charge sheets and normalizing by V_0 to determine direct flux, and (3) determining the total indirect flux by integration of the normal component of the magnetic field over the pole surface and normalizing by V_0 to find the capacitance.

HYBRID UNDULATOR MODEL

In this section, the solution for a hybrid undulator with infinite permeability poles and uniformly magnetized PM blocks (with $\mu = 1$) is presented. Clearly, the symmetry of the problem can be used to find a solution for the potential of the pole surfaces by considering only one quarter of a period on either the top or bottom section of the undulator. However, for the solution of pole or PM block perturbations (see following section) it is desirable to consider a sufficiently large section of the undulator. For example, a pole vertical position perturbation applied to a quarter period model would be equivalent to a change in the gap of the entire device. However, by considering a larger section of the undulator, a vertical position perturbation of a single pole can be analyzed.

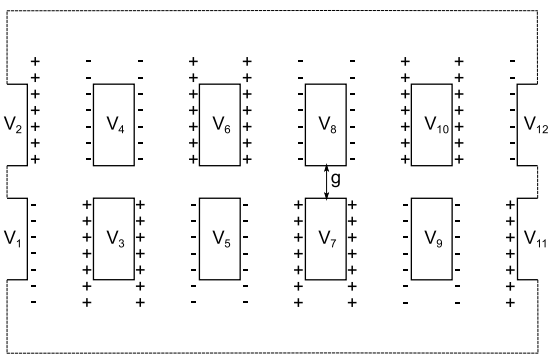

Figure 2: Hybrid undulator model consisting of a number of poles and PM blocks.

Figure 2 shows a diagram of the undulator model that is to be solved. The poles are represented by solid lines which are on a constant scalar potential V_n, where n is the index of each particular pole surface. The PM blocks are represented by charge sheets with charge density $\rho_{eq} = \pm B_r$, where B_r is the remanent field of the PM material. In the diagram, the charge sheets are represented by the $+$ and $-$ symbols for positive and negative charge sheets. On the remaining boundaries (represented by dashed lines in figure 2), the boundary condition $\partial V/\partial n = 0$ is applied.

To obtain a solution to this hybrid undulator model the approach presented in the previous section is used. However, since multiple iso-potential surfaces are considered, the direct and indirect fluxes are represented by vectors while the capacitance is represented by a matrix. For an undulator model with N_p poles the flux balance equation is given by

$$[C]\{V\} = \{\Phi_d\}, \quad (3)$$

where $[C]$ is the $N_p \times N_p$ capacitance matrix, $\{V\}$ is an $N_p \times 1$ vector that contains the scalar potential of each surface V_n, and $\{\Phi_d\}$ is the $N_p \times 1$ direct flux vector. As in the previous section, the direct flux and capacitance are determined from the solution to $\nabla^2 V_i^m = 0$. In this case, the boundary condition $V_i^m(r_m) = V_0$ is applied on one pole surface m while all other pole surfaces are on scalar potential $V_i^m = 0$. The direct flux is then computed using an equation analogous to equation 1 with the subscript and superscript "1" replaced by "m". The components of the capacitance matrix, C_{mn}, are given by, $-\frac{1}{V_0}\int_{\partial\Omega_n} \nabla V_i^m \cdot n da$, which is the flux through pole surface n while surface m is on scalar potential V_0. Note that $[C]$ is a symmetric matrix with $C_{mm} = -\sum_{n \neq m} C_{mn}$, since the total flux into all surfaces must be zero.

PERTURBATION ANALYSIS

In this section a general analysis for pole position and dimension errors and for PM block errors is presented. Starting with a equation 3, a perturbed problem can be written as

$$([C] + [\delta C])(\{V\} + \{\delta V\}) = \{\Phi_d\} + \{\delta\Phi_d\}, \quad (4)$$

where $[\delta C]$ is the perturbation of the capacitance matrix, $\{\delta\Phi_d\}$ is the perturbation to the direct flux, and $\{\delta V\}$ is the perturbation to the equilibrium potential of the poles. PM block errors are characterized by perturbations to the strength or location of charge sheets, which leads to a perturbation of the direct flux term. Pole positioning or dimension errors are characterized by changes in the geometry of the scalar potential surfaces, which lead to a perturbation of the capacitance matrix.

PM Block Perturbation

PM block perturbations are modeled as excess charge sheets, which lead to a perturbation in the direct flux. Figure 3 shows an example where the height of a PM block is too large which leads to longer charge sheets than in the original unperturbed case. The total contribution to the direct flux is then given by the sum of the direct flux in the original problem, $\{\Phi_d\}$, and the direct flux in the perturbed problem, $\{\delta\Phi_d\}$. To compute the m'th component of $\{\delta\Phi_d\}$, $\delta\Phi_d^m$, the solution to the BVP, $\nabla^2 V_i^m = 0$, is obtained with boundary conditions $V_i^m(r_m) = V_0$ on pole

ISBN 978-3-95450-117-5

surface m and $V_i^m = 0$ on all other pole surfaces. Equation 1 is then used, where Ω_ρ is the domain on which the excess charge density lies and the subscript and superscript "1" replaced by "m". The perturbation in the direct flux due to a PM block error will lead to a change in the equilibrium potentials of the undulator poles. The solution to the potential perturbation is given by

$$[C]\{\delta V\} = \{\delta\Phi_d\}, \tag{5}$$

where the higher order term, $([\delta C]\{\delta V\})$, is neglected.

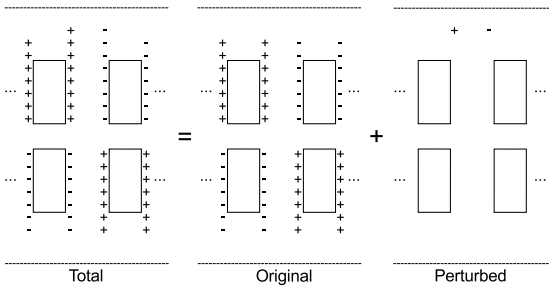

Figure 3: Diagram of a PM block perturbation, which is modeled using excess charge sheets.

Pole Perturbation

Pole perturbations are characterized by geometric changes to the poles, which lead to a perturbation of the capacitance matrix. The perturbation to the capacitance matrix could be determined by generating two solutions (one before the perturbation and one after) and subtracting the capacitance matrix of the second solution from the first. However, this is a cumbersome process since two sets of geometries have to generated and meshed for the BVP solver. Furthermore, a fine mesh may be necessary to capture the differences between the two solutions when small perturbations are performed. A different approach is pursued here, where the geometry of the undulator domain is fixed and the boundary values of the perturbed geometry are modified. This approach relaxes the high density mesh requirement since the perturbation problem can be solved directly, and it circumvents the need to generate multiple meshes.

Figure 4 shows a diagram of the boundary value perturbation approach for geometric perturbations of the iso-scalar potential surfaces. On the left, the total problem is shown which describes the evaluation of one row (or column due to symmetry) of the capacitance matrix. Here, the surface of the upper central pole is modified so that it protrudes further to the right than the original pole. In the calculation of the m'th row of the capacitance, a solution for an indirect scalar potential, $V_i^m(r)$, is obtained with boundary conditions $V_i^m(r_m) = V_0$ on pole surface m and $V_i^m = 0$ on all other surfaces. For a perturbed pole with index n, a first order approximation can be introduced where the new pole geometry is replaced by the original pole geometry. The boundary value on the faces that are shared with the original pole is then set to $V_i^m(r_n) = 0$ for $m \neq n$ and $V_i^m(r_n) = V_0$ for $m = n$, while the remaining face is on a perturbed scalar potential, $V_i^m(r_n) + (\partial V_i^m/\partial x)\delta x$. Here, x is oriented with the perturbation direction, while δx represents the size and direction of the perturbation.

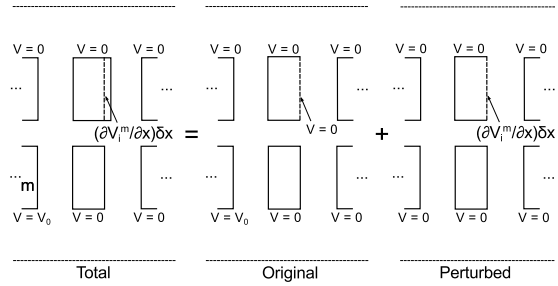

Figure 4: Diagram of the boundary value perturbation approach for pole errors.

The perturbation in the capacitance matrix due to a pole error will lead to a change in the equilibrium potentials of the undulator poles. The solution to the potential perturbation is given by

$$[C]\{\delta V\} = -[\delta C]\{V\}, \tag{6}$$

where once again the higher order term, $([\delta C]\{\delta V\})$, is neglected. Equation 6 can be evaluated by first forming the perturbation capacitance matrix $[\delta C]$, however, it is more convenient to calculate $[\delta C]\{V\}$ directly. As is depicted in the right side of figure 4, the perturbation matrix is determined by setting all surfaces on $V = 0$, except for the perturbed surface which is placed on scalar potential $(\partial V_i^m/\partial x)\delta x$. The m'th component of the vector $[\delta C]\{V\}$ is determined by calculating the indirect flux into surface m with the perturbed surface on scalar potential $\delta x \sum_m \partial V_i^m/\partial x$, while all other surfaces are on potential $V = 0$. Here V_i^m corresponds specifically to the solution of $\nabla^2 V_i^m = 0$ with surface m on prescribed potential $V = V_0^m$ ($V = 0$ for all other surfaces), where V_0^m is the m'th component of the vector obtained from the solution of equation 3. The sum $\sum_m \partial V_i^m/\partial x$ is then given by $B_x^i(r_p)$, where B^i is the total indirect field for the original problem (see figure 2), r_p is the position of points on the perturbed surface, and x is oriented along the direction of the surface perturbation. In summary, the vector $([\delta C]\{\delta V\})$ is determined by calculating the flux through the poles with the perturbed surface on scalar potential $B_x^i(r_p)\delta x$ while all other pole surfaces have prescribed potential $V = 0$.

EXAMPLES

In this section, some examples of the different error perturbations that can be analyzed with this model are presented. Figure 5 shows a limited set of the types of errors that are expected in an undulator. These include: (a) B_r strength errors for the PM blocks, (b) pole position errors

ISBN 978-3-95450-117-5

along the axis, (c) B_r angle errors, and (d) vertical pole position errors. The figure depicts how each of these errors would be analyzed using the model described in this work. For the examples analyzed in the remainder of this work, the following parameters are used: the undulator period is $\lambda_u = 32$ mm, $B_r = 1.32$ T, and the minimum and maximum gap are 7.2 mm and 20 mm respectively. The calculations are performed using the magnetostatic finite element code TOSCA in a two-dimensional setting. However, it is noted that a specialized magnetostatic code is not necessary for this model since only the solution to a BVP for the Laplace equation is required.

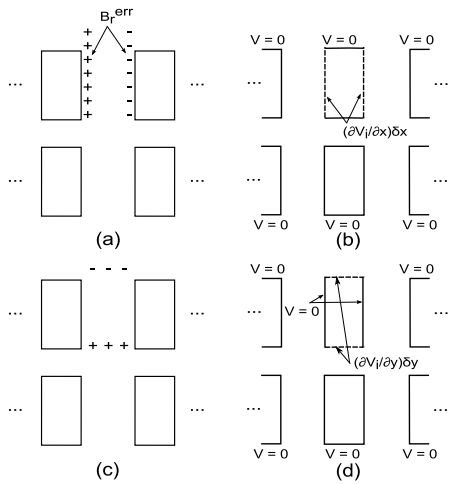

Figure 5: Example of possible types of errors in a hybrid undulator: (a) B_r strength errors for the PM blocks, (b) pole position errors along the axis, (c) B_r angle errors, and (d) vertical pole position errors.

Figure 6 shows the result for the normalized on-axis vertical magnetic field error for a 0.2% block strength error (see (a) in figure 5) at two different gaps (7.2 mm - red line, 20 mm - blue line). The normalization factor is the peak on-axis field at the corresponding gap. The on-axis error field for this example is composed of only indirect fields, which are derived from the calculation of the potential perturbation vector, $\{\delta V\}$. In figure 6 the PM block error is located at $x = 0$ while the poles are located where the local maxima occur in the vertical field.

Figure 7 shows the result for the normalized on-axis vertical magnetic field error for an axial pole position error with a magnitude of 25 μm (see (b) in figure 5) at two different gaps (7.2 mm - red line, 20 mm - blue line). For this example, the on-axis error field is composed of both the indirect fields which are derived from the potential perturbation vector, $\{\delta V\}$, as well as the field that is generated by the perturbed scalar potential surfaces. In this case, the pole error is located at $x = 0$, and the remaining poles are located where the local maxima occur. For both of these examples the field extends out further for the larger gap leading to larger normalized peak magnetic field integral values.

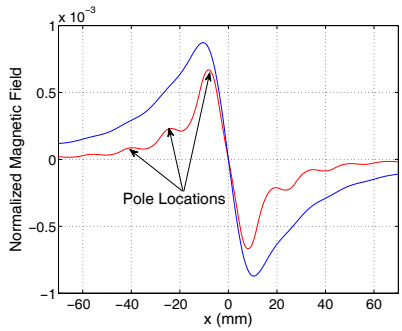

Figure 6: Normalized magnetic field error for a 0.2% block strength error at 7.2 mm (red) and 20 mm (blue) gaps.

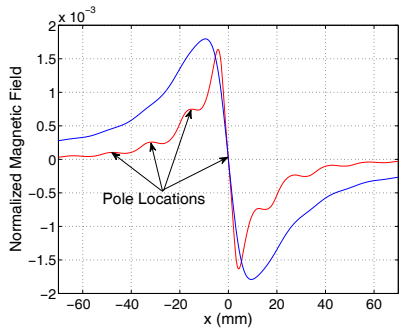

Figure 7: Normalized magnetic field error for a 25 μm axial pole position error at 7.2 mm (red) and 20 mm (blue) gaps.

CONCLUSIONS

In this work, a model is developed to investigate the effect of mechanical and magnetic tolerances on magnetic field errors for hybrid undulators. The approach that is used allows for a large variety errors to be modeled under the same framework. For the examples presented here, a two-dimensional analysis is performed. This restricts the solutions to have zero net on-axis vertical magnetic field integrals for all of the possible errors. However, the modeling framework is general (it only requires a solution to a BVP problem for the Laplace equation) and is not restricted to two-dimensional calculations. The evaluation of the magnetic field errors in a three-dimensional setting will be the subject of future work.

REFERENCES

[1] H.-D. Nuhn, Y.T. Ding, Z.R. Wolf, J. Wu, and S. Marks "LCLS-II undulator tolerance analysis," FEL2011 Conference Proceedings.

[2] K-Halbach, "3-D Hybrid Theory," Law. Berk. Lab. Rep. LBL-034 (1989).

[3] R.D. Schlueter, "Field errors in hybrid insertion devices," Law. Berk. Lab. Rep.LBL-36839 (1995).

[4] R. Savoy, K. Halbach, W. Hassenzahl, E. Hoyer, D. Humphries and B. Kincaid, "Calculation of magnetic error fields in hybrid insertion devices," Nuclear Instruments and Methods in Physics Research Section A. 291, (1990), p. 408.

ISBN 978-3-95450-117-5